Geotextiles and Geomembranes 32 (2012) 18–27

Contents lists available at SciVerse ScienceDirect

Geotextiles and Geomembranes

journal homepage: www.elsevier.com/locate/geotexmem

Long-term lateral displacement of geosynthetic-reinforced soil segmental retaining walls

Huabei Liu*

Department of Civil Engineering, City College of New York/CUNY, 160 Convent Ave., New York, NY 10031, United States

ARTICLE INFO

Article history:
Received 14 June 2011
Received in revised form
21 November 2011
Accepted 6 December 2011
Available online 28 January 2012

Keywords:
Geosynthetic-reinforced segmental walls
Creep
Lateral deformation
Deformation components

ABSTRACT

The service limit-state design of Geosynthetic-Reinforced Soil (GRS) retaining walls requires accurate estimation of the lateral facing displacement at the end of construction as well as after years of creep. However, before a simplistic but rational methodology for this purpose can be developed, mechanisms governing the short-term and long-term lateral facing displacements must be clarified. In this study, extensive Finite Element analyses were carried out using a calibrated Finite Element procedure to investigate and attempt to better understand the lateral facing displacements of segmental GRS walls at the end of construction and after 10 years of creep under constant gravity loading. The study found that among the two main components of lateral facing displacement, the deformation of reinforced soil zone was largely governed by reinforcement spacing and reinforcement stiffness, while the influence of reinforcement length was negligible. Soil stiffness also played an important role in the lateral deformation if large reinforcement stiffness and/or small reinforcement spacing were used. In contrast, reinforcement length to a very large extent determined the lateral displacement at the back of reinforced soil zone. With constant reinforcement length, the reinforced soil zone could be treated as a deep beam. The displacement at the back of reinforced soil zone was then determined by the earth pressure, beam depth, and beam stiffness, the last of which is a function of soil stiffness, reinforcement spacing, reinforcement stiffness, and facing stiffness. The study found that isochrone stiffness can be used to interpret the lateral deformation of GRS walls under working stress condition.

1. Introduction

Geosynthetic-Reinforced Soil (GRS) retaining walls are used extensively as permanent structures in many countries. Safety has always been the first concern in designing earth retaining structures. But the serviceability of permanent earth retaining structures is of equal importance. For permanent GRS retaining walls designed with an expected life of 75–100 years, the "service limit state" is as important as the "strength limit state" and must be checked during the design stage (AASHTO, 2007). For this purpose, AASHTO (2007) and FHWA (Elias et al., 2001) both suggest the empirical method proposed by Christopher (1993), which estimates the maximum lateral displacement of simple GRS walls at the end of construction (EOC). Long-term deformation is not taken into account in this method.

Nonetheless, long-term deformation due to creep cannot be neglected for GRS walls (e.g. Fannin, 2001; Benjamim et al., 2007; Yang et al., 2009). Even using clean granular backfill with small creep, the horizontal displacement of GRS walls can continue to develop due to the time-dependent properties of some geosynthetic reinforcements, such as high-density polyethylene (HDPE) and polypropylene (PP) geogrids (e.g., Allen and Bathurst, 2002; Liu and Ling, 2007; Liu and Won, 2009), although it may be small if polyester (PET) or polyvinyl alcohol (PVA) type of geosynthetics is used (e.g., Kaliakin et al., 2000; Kongkitkul et al., 2010). Besides, the empirical method does not take into account the effects of soil strength or soil stiffness, assuming that well-compacted and high-strength granular soils are used as backfill materials. However, extensive studies have shown that backfill strength and stiffness play critical roles in the lateral displacement of GRS walls (e.g., Rowe and Ho, 1998; Helwany et al., 1999; Ling and Leshchinsky, 2003; Ling et al., 2005).

Simplistic analytical methods also exist for the analyses of reinforced soil structures under working stress condition, some having the capacity to estimate lateral facing displacement (e.g. Ehrlich and Mitchell, 1994; Allen et al., 2003; Klar and Sas, 2009; Correia et al., 2011). But how to address the issue of creep deformation is still not resolved in the existing methods.

* Tel.: +1 212 650 8007; fax: +1 212 650 6965.
E-mail address: hliu@ccny.cuny.edu.

0266-1144/$ – see front matter © 2011 Elsevier Ltd. All rights reserved.
doi:10.1016/j.geotexmem.2011.12.001

Alternatively, numerical methods can accurately estimate lateral deformation of reinforced soil walls, provided that proper models are used to simulate backfill soil, geosynthetics, and soil–structure interaction (e.g., Christopher, 1993; Karpurapu and Bathurst, 1995; Rowe and Ho, 1998; Helwany et al., 1999, 2007; Rowe and Skinner, 2001; Ling and Leshchinsky, 2003; Ling et al., 2004; Hatami and Bathurst, 2006; Guler et al., 2007; Yoo and Kim, 2008; Ling and Liu, 2009). With proper modeling of the time-dependent properties of soils and/or geosynthetics (e.g., Hirakawa et al., 2003; Kongkitkul et al., 2004, 2007; Liu and Ling, 2005, 2007; Yeo and Hsuan, 2010), the long-term deformation of reinforced soil structures can also be captured by numerical methods (e.g., Helwany and Wu, 1997; Li and Rowe, 2001, 2008; Skinner and Rowe, 2003, 2005; Rowe and Taechakumthorn, 2008; Bergado and Teerawattanasuk, 2008; Liu and Won, 2009; Liu et al., 2009; Li et al., 2011).

In this study, a Finite Element procedure that was calibrated for long-term behavior of reinforced soil structures as per Liu and Won (2009) was employed to investigate the end of construction (EOC) and long-term deformations of geosynthetic-reinforced segmental retaining walls under working stress condition. The study attempts to understand the deformation mechanisms so that a simplistic methodology can be developed in the future to estimate lateral facing displacement for the purpose of service limit-state design. Only granular backfill soil was considered in this study, which was assumed to be time-independent, and no surcharge was applied on the backfill surface of retaining walls. The walls were analyzed for 10 years of creep under constant gravity loading following the end_of_construction (EOC).

2. Finite element procedure and models

The plane-strain Finite Element procedure in this study was reported in Liu and Won (2009). The modified version of Swndyne II (Chan, 1993; Liu, 2002) was used in this study. The procedure consists of two steps, the first of which simulates the construction of GRS retaining walls, while the second models their creep responses following the end of construction (EOC). It was validated for construction simulation in Ling et al. (2004) and Ling and Liu (2009), while its creep simulation capacity was validated against a model test on sand–geotextile composite reported in Wu and Helwany (1996).

In this procedure, time-independent granular backfill soil is assumed and modeled by a generalized plasticity model for sand (Ling and Liu, 2003). The geosynthetic reinforcement is simulated by a elastoplastic viscoplastic bounding surface model that is capable of describing nonlinear, creep and stress relaxation responses of geosynthetics under 1D tensile loading (Liu and Ling, 2005, 2007). Under working stress condition, slippage between geogrid, which is the type of reinforcement considered in this study, is expected to be minimal (Ling et al., 2005), hence perfect bounding is assumed between backfill soil and reinforcement. However, slip elements (Chan, 1993), which express the slippage of soil–structure interfaces following Mohr–Coulomb criterion, are used to model the interfaces between backfill soil and facing blocks as well as those between facing blocks. Appendices I and II briefly introduce the constitutive models for soil and geosynthetics, details of which can be found in Ling and Liu (2003) and Liu and Ling (2005, 2007).

Three wall heights, 6 m, 8.2 m and 10 m, were analyzed. All of the walls had vertical modular-block facings, and were constructed on a 3-m stiff foundation of very dense granular soils (Lee and Seed, 1967). Geogrid reinforcement layers were assumed to be perfectly pinned to the facing blocks. Finite element meshes of all model walls extended 32 m behind the facing blocks so that the boundary effects would be minimized. They were fixed at the base and had roller boundaries on both sides. Fig. 1 shows part of the Finite Element mesh of an 8.2-m wall. The construction of the model walls was assumed to be fast, with the 6-m walls completed in 10 days, the 8.2-m walls completed in 14 days, and the 10-m walls completed in 17 days.

The Finite Element procedure does not take into account the effect of compaction on lateral deformation during construction. Construction sequence was simulated by activating layers of Finite Elements steps by steps. The thickness of each increment was 20 cm, the same height as the facing block. No additional pressure was applied on the element layers to simulate compaction pressure. Neglecting of compaction effect may underestimate lateral deformation if the retaining wall is low. However, when the retaining wall is sufficiently high, such as those investigated in this study, the compaction effect would be limited to the upper portion of the retaining wall (Bathurst et al., 2009). Since maximum facing displacement is the main concern of service limit-state design and the focus of the present study, which generally occurs at the mid-height of the retaining wall, the assumption would have small influence on the conclusion of the study. It is noted that most design and construction codes of GRS walls require the use of small compaction machine in the area close to the facing in order to limit the compaction induced lateral facing displacement. Finite element procedures following similar construction sequence simulation have also been shown to be able to model the lateral displacement of medium to high GRS walls that are constructed according to the code requirements (e.g. Ling and Leshchinsky, 2003; Ling et al., 2004).

In the present study, the facing blocks were placed directly on the foundation soil and perfect bounding was assumed between them. But the blocks together with the reinforced soil zone were allowed to slide if the backfill earth pressure was sufficiently large and exceeded the shear resistance of foundation soil. This assumption is close to reality since facing blocks are placed on leveling pad and allowed to slide. There may be a small passive earth pressure in front of the wall if a small thickness of fill is present in front of the wall, which was partly taken into account by assuming perfect bonding between facing block and foundation soil. Segmental reinforced soil walls cannot be assumed to be fixed at the base since even stiff soils have limited shear resistance.

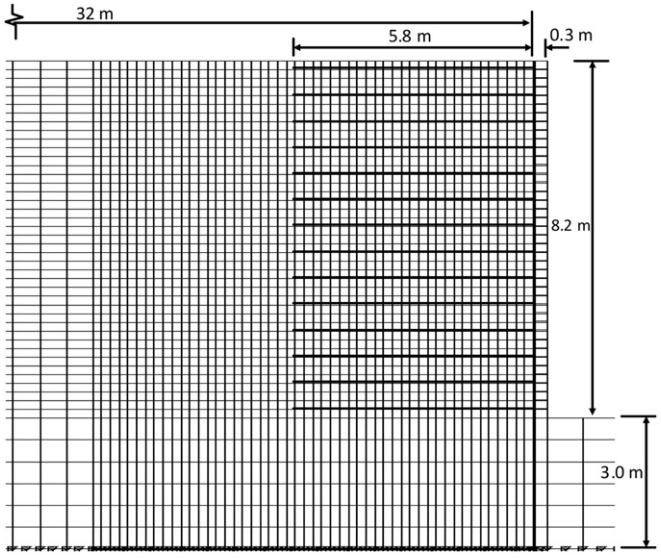

Fig. 1. Part of one finite element mesh.

A fixed base would artificially increase the shear resistance at the base of facing blocks and reduce the load that should have been carried by reinforcement layers, particularly the lower ones (Ling and Leshchinsky, 2003; Leshchinsky, 2009). Extensive analysis was carried out on a wide range of model geosynthetic-reinforced segmental walls in order to obtain a more comprehensive understanding of their long-term lateral deformations. For each wall height, reinforcement length ratios ranging from 0.6*H* to 1.2*H* were analyzed, and for each reinforcement length, the effects of reinforcement spacing, backfill soil, and reinforcement stiffness were investigated. Altogether more than 170 cases were analyzed, as shown in Table 1. The effects of backfill soils were investigated using medium loose Sacramento River sand (Lee and Seed, 1967), a Japanese silty sand (Ling et al., 2004), dense Toyoura sand (Fukushima and Tatsuoka, 1984) and dense Sacramento River sand (Lee and Seed, 1967). Their model parameters and their stress–strain relationships at $\sigma_3 = 30$ kPa under triaxial compressions are shown in Appendix I, while their parameter calibrations can be found in Liu (2002) and Ling and Liu (2003). The friction angles of these soils at $\sigma_3 = 30$ kPa under triaxial compressions are approximately 37°, 40°, 44°, and 47°, respectively. The effects of reinforcement stiffness were investigated using the five geogrids shown in Appendix II. Among them, Grid II was an actual HDPE geogrid, the parameters of which were calibrated in Liu and Ling (2005, 2007), while the other four were model geogrids, the parameters of which were obtained by varying those of Grid II. Fig. (14) in Appendix II shows the isochrones of the geogrids at 14 days and 10 years, respectively.

The concrete facing block was assumed to be linear elastic with Young's modulus $E = 2000$ MPa and Poisson's ratio $\nu = 0.17$ and have a dimension of 30 cm by 20 cm. Its unit weight was assumed to be 18 kN/m^3, considering that it is usually hollow and filled with gravel. The interface between blocks was modeled using slip elements with $\delta = 19.5°$ and $c = 0.5$ kPa (Ling et al., 2004), while the interface between soil and facing blocks was assumed to have a friction angle of $\delta = \tan^{-1}(0.67 * \tan\phi)$, with ϕ being the friction angle of backfill soil. It is understood that the backfill soils have different unit weights. However, in order to focus on the effects of soil strength and soil stiffness, the unit weights of all backfill soils were assumed to be 17.5 kN/m^3, which is the unit weight of Soil IV with a low water content.

3. Component of lateral facing displacement

As summarized in Rowe and Ho (1998), without surcharge, lateral facing displacement consists of the contributions from deformation of reinforced soil zone (RS zone), displacement at the back of reinforced soil zone, displacement due to foundation yielding (Skinner and Rowe, 2003, 2005; Rowe and Taechakumthorn, 2008; Bergado and Teerawattanasuk, 2008; Li and Rowe, 2008; Viswanadham and König, 2009; Huang and Luo, 2010; Rowe and Taechakumthorn, 2011), compaction (e.g., Hatami and Bathurst, 2006; Bathurst et al., 2009), slack in reinforcement connection, and dislocation of facing blocks. With proper quality control, slack in reinforcement connection and block dislocation can be minimized. While compaction may have considerable effect on the displacement of facing close to the roller, its effect will be mostly offset by overburden soil pressure if the retaining wall is high and it will only affect the displacement at the very upper portion of the wall at the end of wall construction and beyond (Ling et al., 2004; Bathurst et al., 2009). With these factors taken into account, the lateral facing displacement of medium-high to high segmental GRS walls mainly comes from the deformation of reinforced soil zone, the displacement at the back of reinforced soil zone and the additional effect of foundation yielding. The present study focuses on retaining walls constructed on firm foundation, which is mostly the case in practice (Elias et al., 2001).

For GRS walls constructed on firm foundations, reinforced soil deformation and displacement at the end of reinforced soil zone are the two main contributions to facing displacement, as can be seen in Fig. 2, which shows the results of a 6-m high wall using base-case wall parameters. Under working stress conditions, the deformation of segmental GRS walls can be considered as the internal lateral deformation of a deep reinforced soil "beam" together with its deflection and translation due to the earth pressure acting at its back. Due to the viscous properties of HDPE or PP geosynthetic reinforcement, the facing displacement might increase, particularly in the mid and upper portion. The increase was attributed to the increase of reinforced soil deformation as well as the decrease of reinforced soil stiffness in the upper portion that resulted in larger lateral displacement at the back of RS zone. The decrease of reinforced soil stiffness in the upper portion of reinforced soil zone was attributed to the increase of soil stress in this region, as explained in Liu and Won (2009). Fig. 2 also shows that the RS zone as a whole translated slightly under the backfill earth pressure. Due to the large shear strength and high stiffness of foundation soil, no foundation yielding or large settlement was observed in all the cases. The small lateral displacement at the base of the reinforced soil zone was attributed to the shear deformation of foundation soil directly beneath the reinforced soil zone under backfill earth pressure.

Table 1
Analyzed cases.

Wall height	Reinforcement length	Base case	Reinforcement spacing	Backfill soil	Reinforcement
6 m	3.4 m 3.8 m 4.2 m[a] 5 m 6 m 7.2 m	Sv = 0.6 m, Soil II, Grid II	Sv = 0.2–1.0 m	Soil I to Soil IV	Grids I–V
8.2 m	4.8 m 5.8 m 8.2 m 9 m 9.8 m	Sv = 0.6 m, Soil III, Grid II	Sv = 0.2–1.0 m	Soil I to Soil IV	Grids I–V
10 m	6 m 7 m 10 m 12 m	Sv = 0.6 m, Soil III, Grid II	Sv = 0.2–0.8 m	Soil III and Soil IV	Grids I–V

[a] Additional cases were analyzed with Sv = 0.4 m with varying backfill soil, Sv = 0.8 m.

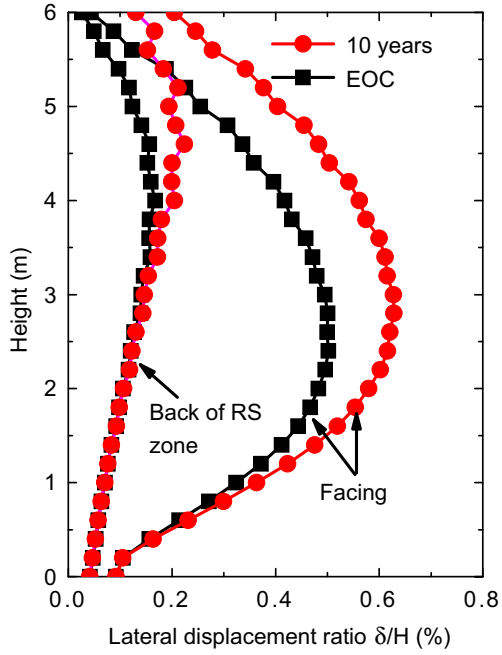

Fig. 2. Lateral displacements ($H = 6$ m with base-case wall parameters).

Due to space constraints, only one case is shown in Fig. 2 but all of the analyzed cases demonstrated similar deformation patterns. It is noted that the mode of long-term facing displacement shown in Fig. 2 was also founded in full-scale field tests (e.g. Onodera et al., 2004).

Fig. 3 shows the ratio of maximum displacement δ_b^{max} at the back of RS zone to maximum facing displacement δ^{max} for various L/H ratios. As can be expected, the ratio decreased with an increase in the reinforcement length, and for all of the cases analyzed, the decrease followed the trend of some exponential function regardless of wall height. Fig. 3 also shows that the displacement ratio was related to reinforcement stiffness, reinforcement spacing and backfill soil, which is easy to understand if we consider the RS zone as a deep beam that deflects under backfill earth pressure. These three factors all influenced the stiffness of the deep beam and/or the backfill earth pressure. Generally speaking, lower-stiffness reinforcement led to smaller displacement ratio, but with $L = 0.7H$ and Sv = 0.6 m, which represents normal reinforcement layout, the EOC and long-term displacement ratios can still be as large as 20–30% and cannot be neglected in lateral displacement estimation.

Fig. 4 shows the lateral earth pressures at the back of the reinforced soil zone of some cases ($H = 6$ m). The lateral earth pressure was generally larger than the Rankine's active earth pressure at the end of construction (EOC), as can be expected since the deflection of the reinforced soil zone was not large enough to mobilize active earth pressures. But the earth pressures slightly decreased in the upper portion due to the increase of deflection. Note that the Rankine's active earth pressure was obtained using a triaxial friction angle, which was smaller than the plane-strain one. This explains why after 10 years of creep, some earth pressures were smaller than the Rankine values in the upper portion of the wall. The earth pressure also increased with an increase in reinforcement length and reinforcement stiffness, and with a decrease in reinforcement spacing, but the earth pressures were between the active earth pressure and the at-rest earth pressure for all the cases analyzed.

It is clear that, in order to estimate facing displacement of segmental GRS walls under working stress conditions, both the deformation of reinforced soil zone and the displacement at the back of reinforced soil zone must be properly considered. The following sections investigate the patterns and mechanisms of these two components, with the objective of shedding some light on this important issue.

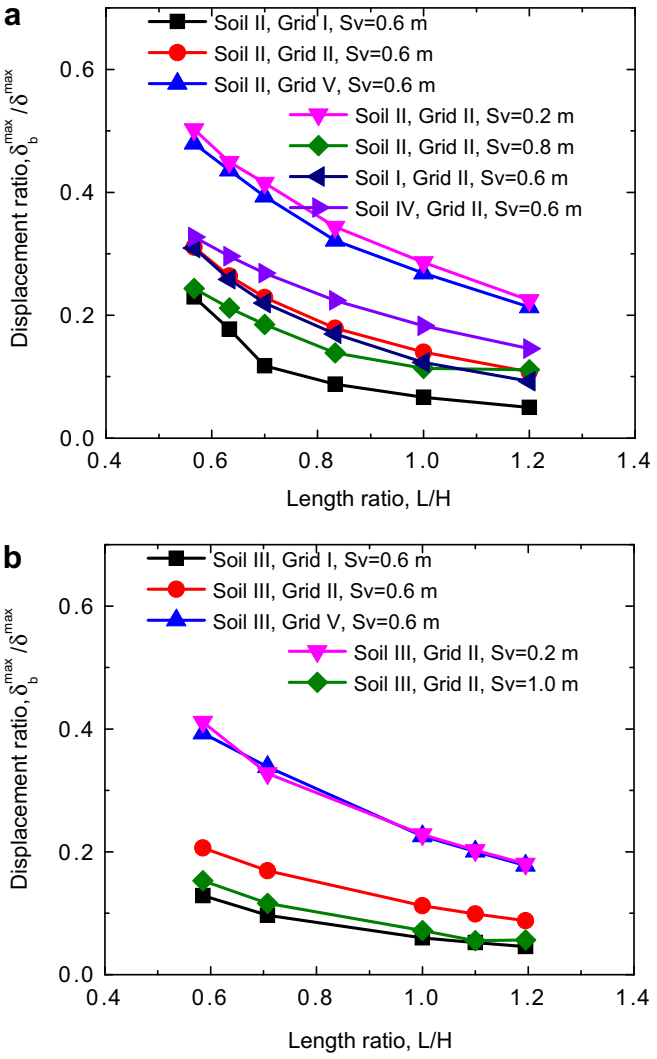

Fig. 3. Lateral displacement ratios after 10 years of creep: (a) $H = 6$ m; (b) $H = 8.2$ m.

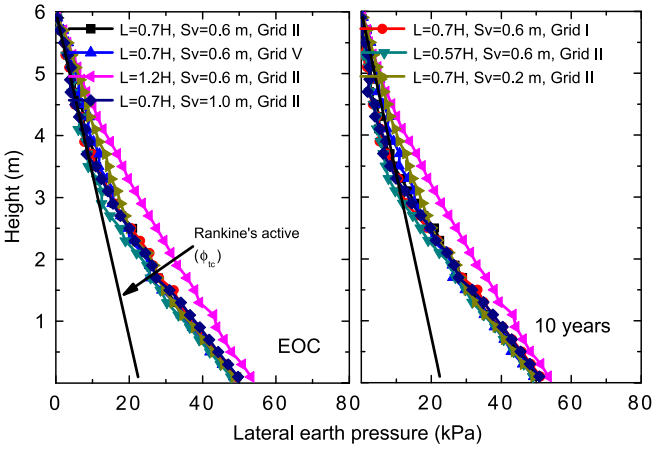

Fig. 4. Lateral earth pressures behind the back of the reinforcement soil zone.

4. Lateral deformation of reinforced soil zone

The important factors that determined the lateral deformation of the reinforced soil zone were backfill soil, reinforcement spacing and reinforcement stiffness. Reinforcement length only had a small influence on the maximum lateral deformation of the reinforced soil zone unless it is improperly short.

Fig. 5 shows the relationship between maximum lateral deformation δ_{RS}^{max} of reinforced soil (RS) zone at EOC, or maximum creep $\Delta\delta_{RS}^{max}$ increase after 10 years, and reinforcement length ratio L/H with different backfill soils. The EOC deformation increased slightly with reinforcement length while the creep decreased slightly. This trend is not difficult to understand since reinforcement load was only slightly related to reinforcement length when it is greater than $0.6H$ (e.g., Ling and Leshchinsky, 2003; Ling et al., 2005; Liu and Won, 2009), which was the case in this study, and the zone of zero reinforcement load is only related to the friction angle (the angle of repose) (Rowe and Ho, 1998). Inside the active soil zone, the lateral soil deformation would be similar regardless of reinforcement length; while between zones of active soil state and zero reinforcement load, there was only small difference in deformation due to the small reinforcement load.

In contrast, reinforcement spacing to a large extent determined the reinforced soil deformation. As can be seen in Fig. 6, the lateral deformation of the RS zone increased almost linearly with reinforcement spacing at EOC, so was the creep increase after 10 years. This was consistent with the fact that maximum reinforcement load increased linearly with reinforcement spacing at EOC and under constant loading during wall service (e.g., Rowe and Ho, 1998; Ling and Leshchinsky, 2003; Ling et al., 2005; Liu and Won, 2009).

A similar statement can also be made regarding the effect of reinforcement stiffness, and the effect of reinforcement stiffness and spacing can be unified using the global stiffness $S_{global} = \sum J_i/H$ (Allen et al., 2003; Liu and Won, 2009), in which J_i is the stiffness of a reinforcement layer and H is the wall height. Since the reinforcement is nonlinear, a reference strain of $\varepsilon = 2\%$ was used to obtain the isochrone stiffnesses at 14 days and 10 years, respectively (Fig. (14)). It is understood that the reinforcement strain was not the same in different cases, which would explain some variations of the results. As shown in Fig. 7 for the 6-m high walls, the lateral deformations were very closely related to the

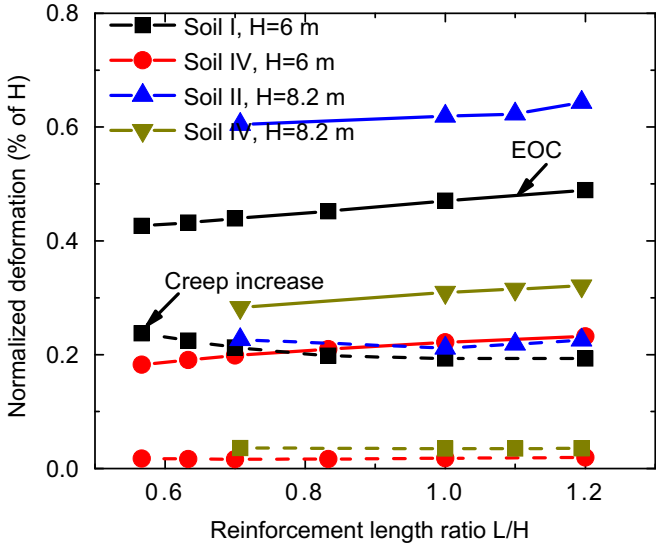

Fig. 5. Effects of reinforcement length on the lateral deformation of RS zone.

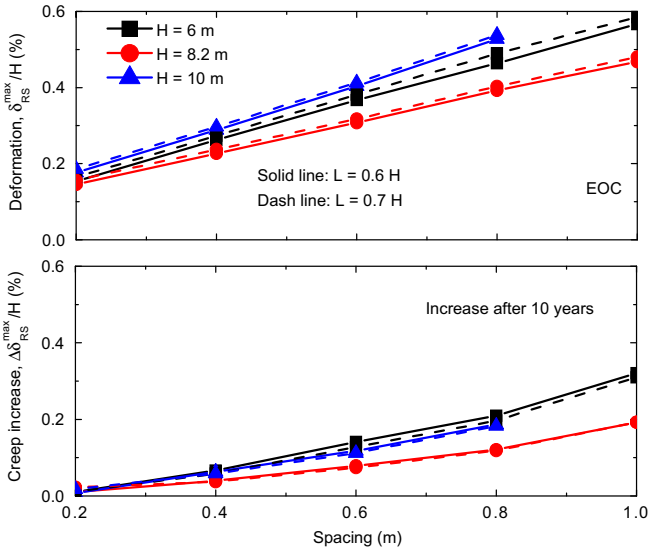

Fig. 6. Effects of reinforcement spacing on lateral deformation of RS zone.

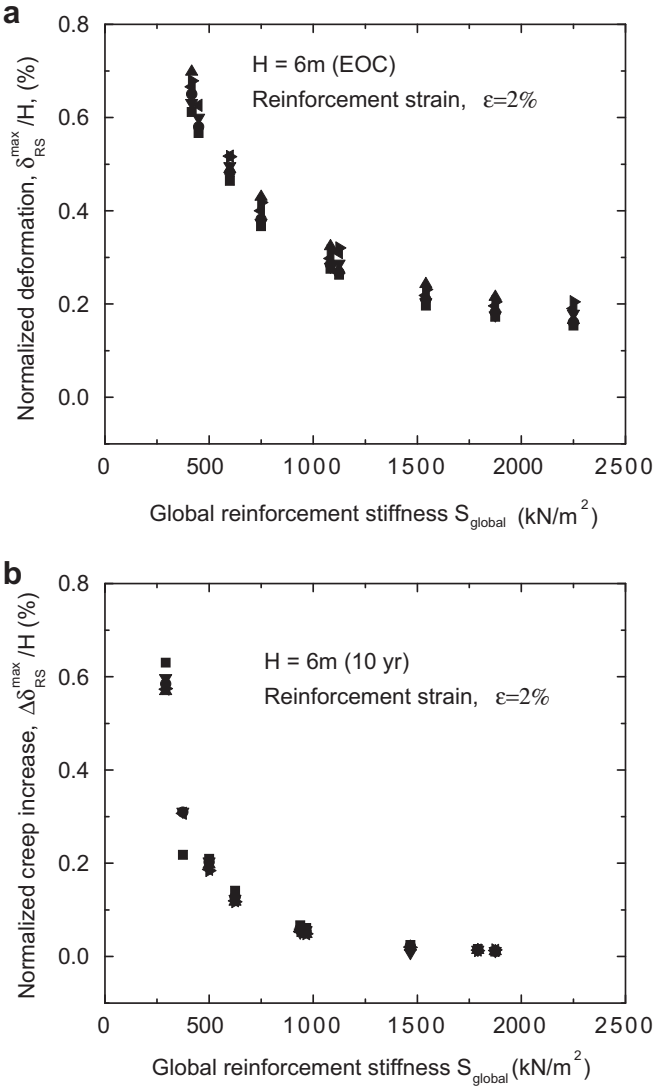

Fig. 7. Effects of global reinforcement stiffness on the lateral deformation of RS zone: (a) EOC; (b) Creep increase after 10 years.

global stiffness through a certain power function. Similar trends were obtained for the other two wall heights but are not presented herein due to space constraint.

Regarding the effects of backfill soils, traditionally it was believed that soil strength or active earth pressure coefficient K_a plays a more important role on lateral deformation than soil stiffness (e.g., Jewell and Milligan, 1989; Rowe and Ho, 1998). This may be the case when low-stiffness reinforcement is used with large spacing, for which the soil deformation is adequately large to mobilize the soil strength. However, with large reinforcement stiffness and/or small reinforcement spacing, soil strength would not be well related to lateral deformation of reinforced soil zone. Fig. 8 shows the relationships between reinforced soil deformation and Rankine's active earth pressure coefficient for various reinforcement stiffnesses and reinforcement spacings. For the cases highlighted in the figure, although the active earth pressure coefficients were quite different, the reinforced soil deformations were similar when the reinforcement was stiff (Grid IV) or the reinforcement spacing was small (Sv = 0.4 m). The effects of soil strength were reflected when the soil stress was large due to either larger reinforcement spacing, smaller reinforcement stiffness, or higher wall height.

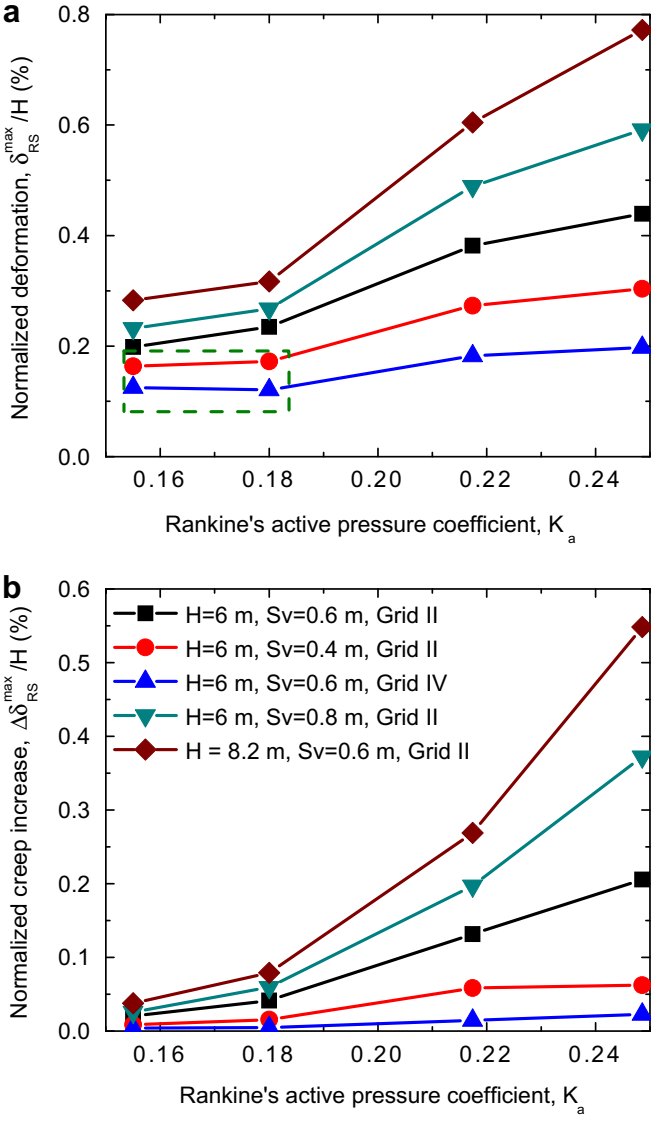

Fig. 8. Effects of backfill soil on the lateral deformation of RS zone: (a) EOC; (b) Creep increase after 10 years.

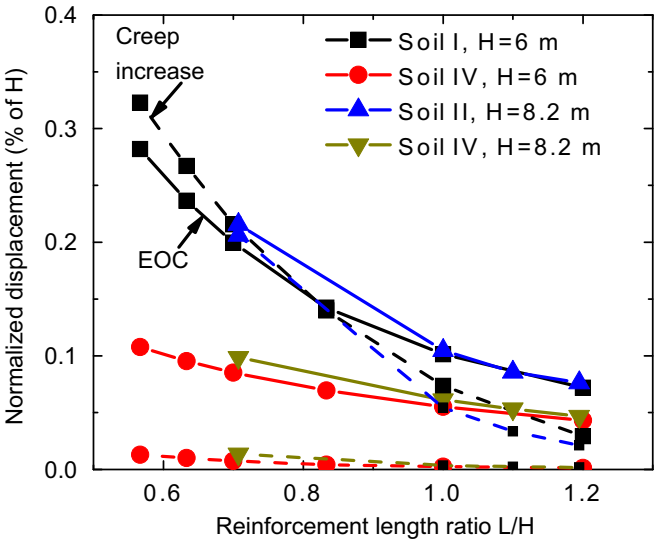

Fig. 9. Effect of reinforcement length on the lateral displacement at the back of RS zone.

5. Lateral displacement at the back of reinforced soil zone

As can be expected, the lateral displacement δ_b^{max} at EOC or the creep increase $\Delta\delta_b^{max}$ after 10 years at the back of the reinforced soil zone is basically determined by reinforcement length L, as shown in Fig. 9. With an increase in the reinforcement length, the lateral displacement at the back of the reinforced soil zone decreased significantly. The decrease was also related to backfill soil stiffness, reinforcement stiffness and reinforcement spacing, as shown in Figs. 3 and 9.

Decrease of reinforcement vertical spacing increased the stiffness of the reinforced soil zone, resulting in smaller lateral

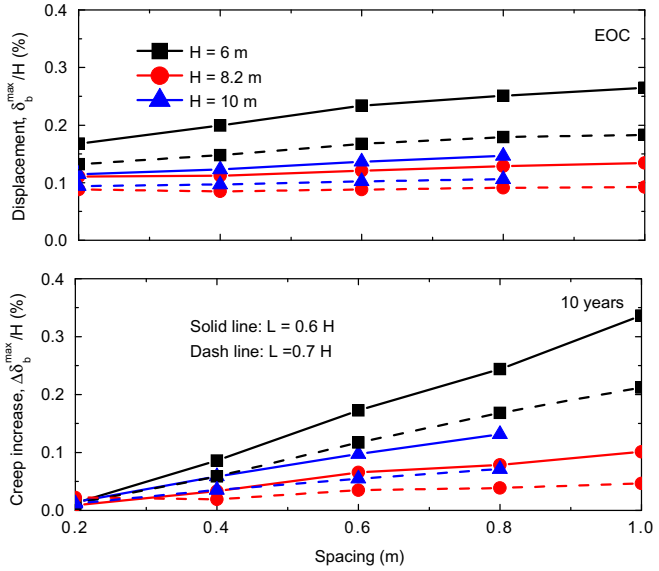

Fig. 10. Effect of reinforcement spacing on the lateral displacement at the back of RS zone.

displacement, as shown in Fig. 10. Like the deformation of the reinforced soil zone, the lateral displacement at its back was also approximately related to reinforcement spacing through a linear function. Increase of reinforcement stiffness had similar effect on the lateral displacement, but the relationship is no longer linear. Similarly, we can also unify the effects of reinforcement stiffness and reinforcement spacing through the global stiffness S_{global}, as shown in Fig. 11. The variation in some of the results is believed to come from the different reinforcement strains in different cases.

Finally the effects of backfill soil are two-fold: it influenced the stiffness of the reinforced soil zone, as well as the magnitude of earth pressure behind the reinforced soil zone. In some cases, the decrease of soil strength also resulted slight decrease in the lateral displacement, as shown in Fig. 12a, which is due to the fact that Soil III and Soil IV had very similar stiffnesses at small strain, but Soil IV resulted in smaller lateral earth pressure due to its larger strength. It can be seen that both soil strength and stiffness should be considered while analyzing the lateral displacement at the back of reinforced soil zone.

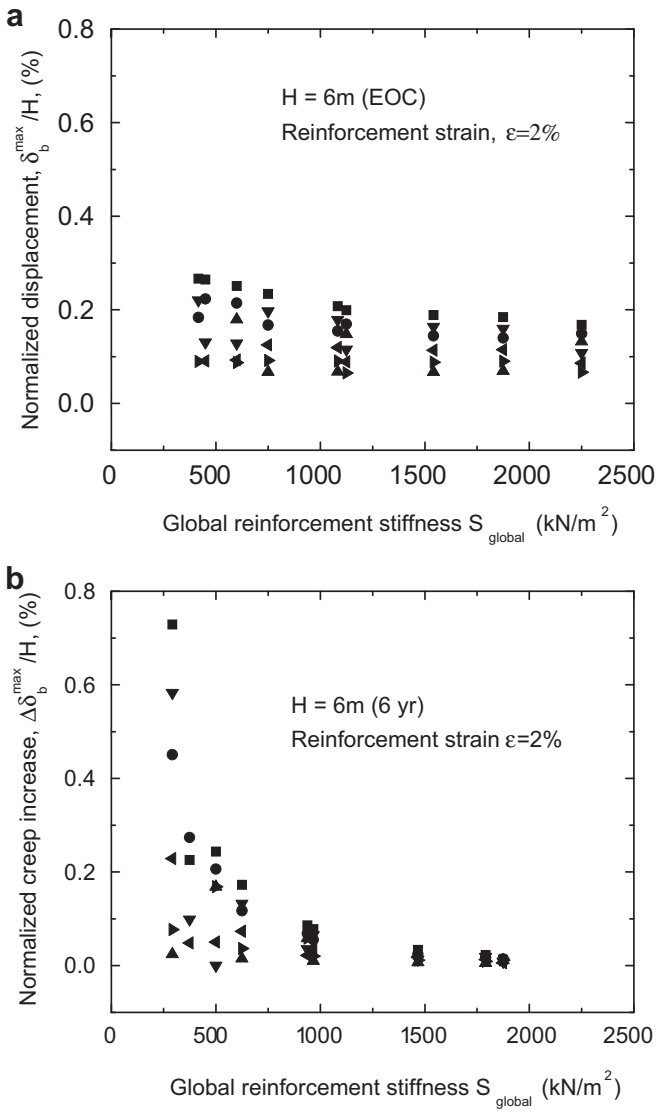

Fig. 11. Effect of global stiffness on the lateral displacement at the back of RS zone: (a) EOC; (b) Creep increase after 10 years.

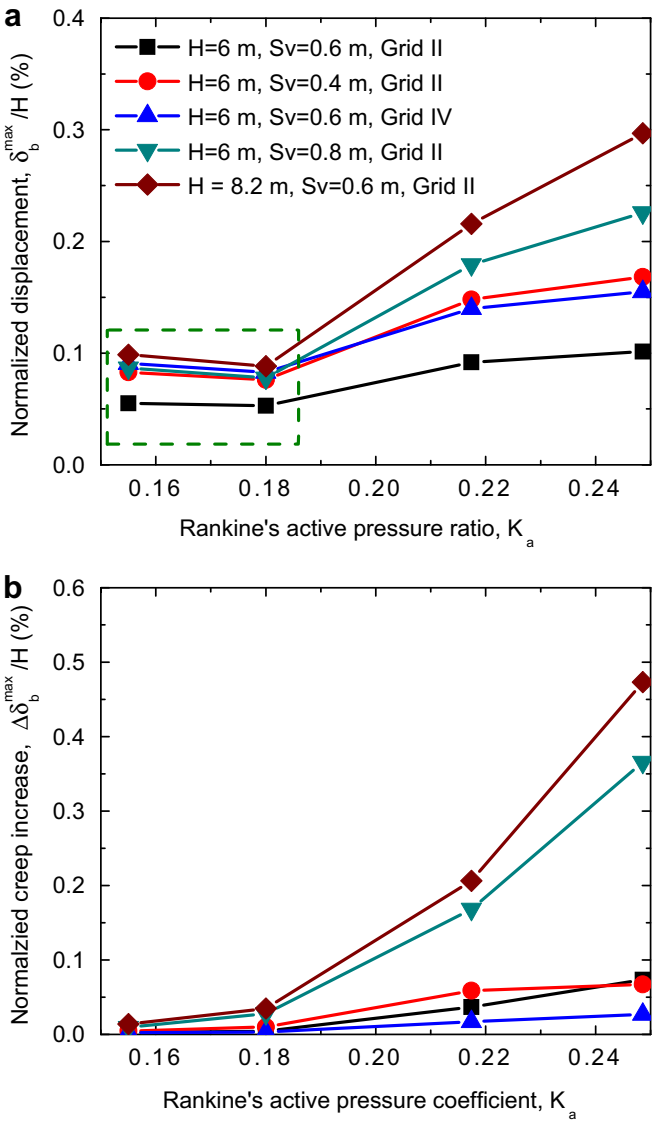

Fig. 12. Effects of backfill soil on the lateral displacement at the back of RS zone: (a) EOC; (b) Creep increase after 10 years.

6. Discussions and conclusions

Extensive Finite Element analyses were carried out using a calibrated Finite Element procedure to investigate the lateral facing displacements of segmental GRS walls at the end of construction and after 10 years of creep under constant gravity loading. No surface surcharge was considered in this study. The objective of this study was to clarify the main components of lateral facing displacement if the GRS walls are constructed on sound and firm foundations, as well as to understand the mechanisms of these deformation components, so that a simplistic methodology can be developed in the future to estimate lateral facing displacement for the purpose of service limit-state design.

It was found that deformations of reinforced soil zone and displacement at the back of reinforced soil zone are the two main components of lateral facing displacement for medium-high to high GRS walls. The deformation of reinforced soil zone was only slightly affected by reinforcement length, but was largely determined by reinforcement spacing and reinforcement stiffness that can be unified by the global reinforcement stiffness $S_{global} = \sum J_i/H$. Soil stiffness played an important role in the lateral deformation when

soil strength was not mobilized owing to large reinforcement stiffness and/or small reinforcement spacing (Leshchinsky and Vulova, 2001). Soil strength took over as the important role when soil deformation was large due to higher soil stress because of low-stiffness reinforcement, large reinforcement spacing or high retaining wall.

In contrast, reinforcement length to a very large extent determined the lateral displacement at the back of the reinforced soil zone. With constant reinforcement length, the reinforced soil zone could be considered as a deep beam, the deflection of which was the lateral displacement at its back. The deflection was determined by the earth pressure as well as the depth and stiffness of the deep beam, the latter of which was a function of soil stiffness, reinforcement stiffness, reinforcement spacing and facing stiffness. Both soil strength, which determines earth pressure, and soil stiffness, which affects beam stiffness, must be considered to estimate the lateral displacement at the back of the reinforced soil zone.

This study and the previous one (Liu and Won, 2009) found that isochrone stiffness can be used to interpret the reinforcement load and lateral deformation of GRS walls under working stress condition. This is because under working stress condition reinforcement load, compared to reinforcement strength, is small and the concept of isochrones is valid (Kaliakin et al., 2000). This finding provides a possibility to estimate the long-term deformation of GRS walls without having to consider the complicate stress redistribution under constant gravity loading (Liu and Won, 2009; Liu et al., 2009).

The present study did not consider the effect of compaction hence the conclusion is probably valid only for retaining walls constructed by low energy compaction. For the medium-high to high GRS walls investigated herein, compaction following the requirement of many construction guidelines (e.g. Elias et al., 2001) is expected to affect only the displacement at the upper portion of a GRS wall (e.g., Bathurst et al., 2009). The maximum lateral displacement that occurs at approximately the mid-height would not have been significantly affected by compaction. The yielding of soft foundation soil was also not considered in this study, but its significance has been extensively investigated by other researchers (Skinner and Rowe, 2003, 2005; Rowe and Taechakumthorn, 2008, 2011; Bergado and Teerawattanasuk, 2008; Li and Rowe, 2008; Viswanadham and König, 2009; Huang and Luo, 2010). Besides, most GRS walls are constructed on firm foundations (Elias et al., 2001).

The present study assumed that the geosynthetic reinforcements exhibited non-negligible viscous response under constant loading. HDPE and PP types of geosynthetics belong to this category. However, PET and PVA geosynthetics have much smaller creep deformation hence the long-term displacement of GRS walls using these reinforcements and granular backfill soils would have much smaller creep displacement increase. Nonetheless, the aforementioned conclusions regarding the EOC displacement mechanisms are still valid.

Acknowledgment

The author would like to thank Professor A.H.C. Chan of Birmingham University for allowing the use of Swandyne-II for this study.

Appendix I

In the generalized plasticity model for sandy soils, the flow direction vector $\mathbf{n}_g$, the loading-direction vector $\mathbf{n}$, and the plastic modulus H are defined explicitly. Nonlinear elastic shear and bulk moduli are firstly written as

$$G_{max} = G_0(p'/p_{atm})^{0.5} \tag{I.1}$$

$$K_{max} = K_0(p'/p_{atm})^{0.5} \tag{I.2}$$

where p' is the present effective confining pressure, p_{atm} is the atmosphere pressure, G_0 and K_0 are model parameters.

The plastic-flow direction vector $\mathbf{n}_g$ in triaxial space is expressed as

$$\mathbf{n}_g = \left(\frac{d_g}{\sqrt{1+d_g^2}}, \frac{1}{\sqrt{1+d_g^2}}\right)^T \tag{I.3}$$

where the dilatancy ratio is assumed to be rated to the stress ratio $\eta = q/p'$ through the following relationship:

$$d_g = \frac{d\varepsilon_v^p}{d\varepsilon_s^p} = (1+\alpha)(M_g - \eta) \tag{I.4}$$

Here, M_g is the slope of the critical state line on p'–q plane, $M_g = 6\sin\phi_{cr}/(3-\sin\phi_{cr}\sin 3\theta)$, ϕ_{cr} is the angle of internal friction at critical state, θ is the Lode's angle, and α is a model parameter.

The constitutive model assumes non-associated flow rule and the loading-direction vector in triaxial space is expressed as:

$$\mathbf{n} = \left(\frac{d_f}{\sqrt{1+d_f^2}}, \frac{1}{\sqrt{1+d_f^2}}\right)^T \tag{I.5}$$

in which

$$d_f = (1+\alpha)\left(M_f - \eta\right) \tag{I.6}$$

The plastic modulus under monotonic loading is defined as:

$$H_L = H_0(p'/p_{atm})^{0.5}\left(1-\frac{\eta}{\eta_f}\right)^4\left\{1-\frac{\eta}{M_g}+H_s\right\} \tag{I.7}$$

where

$$H_s = \beta_{10}\left(\frac{\eta_p/M_g - 1}{M_0}\right)\exp(-\beta_0\xi)\exp\{k_s(p'/p_{atm}-1)\} \tag{I.8}$$

Here ξ is the accumulative plastic deviatoric strain, and $M_0 = \eta_{p0}/M_g - 1$. η_{p0} is η_p at the reference pressure p_{atm}, while the peak stress ratio η_p

Table 2
Model parameters for soils.

	ϕ_0 (°)	$\Delta\phi$ (°)	M_g	M_f	G_0 (kPa)	K_0 (kPa)	k_s	β_{10}	β_0	α	H_0 (kPa)
Soil I	36	2.44	1.3	0.55	55,400	67,700	0.042	0.5	7	0.45	300,000
Soil II	39.4	0.5	1.4	0.645	61,500	67,700	0.1	3.1	20	0.47	50,000
Soil III	43.7	4.9	1.25	0.688	86,100	88,600	0.015	1.1	15	0.5	500,000
Soil IV	44.4	6.5	1.3	0.736	86,100	110,000	0.016	0.6	8	0.45	1,000,000

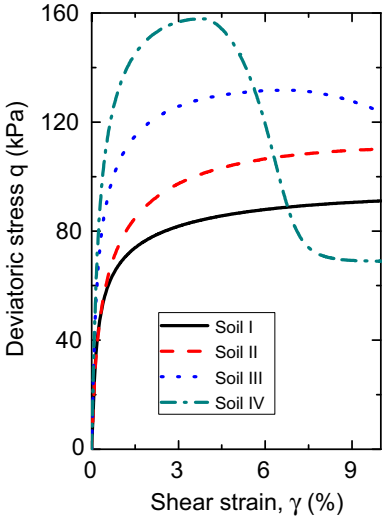

Fig. 13. Stress–strain relationships of soils.

$$\eta_p = \frac{6\sin\phi}{3-\sin\phi\sin 3\theta} \tag{I.9}$$

and

$$\phi = \phi_0 - \Delta\phi\log_{10}(p'/p_{atm}) \tag{I.10}$$

The model requires 11 model parameters to describe the monotonic response of sandy soils. Table 2 shows the model parameters for the fours soils used in this study and Fig. 13 shows their stress–strain relations in triaxial compression at $\sigma_3 = 30$ kPa (Liu, 2002; Liu and Won, 2009).

Appendix II

In Liu and Ling (2005, 2007), a constitutive model was proposed to describe the elastoplastic and viscoplastic responses of geosynthetic reinforcement, in which the total strain rate is expressed as:

$$\dot{\varepsilon} = \dot{\varepsilon}^e + \dot{\varepsilon}^p + \dot{\varepsilon}^{vp} \tag{II.1}$$

Here $\dot{\varepsilon}^e$, $\dot{\varepsilon}^p$, and $\dot{\varepsilon}^{vp}$ represent the elastic, plastic and viscoplastic strain rates, respectively.

The elastic strain rate $\dot{\varepsilon}^e$ is calculated as $\dot{\varepsilon}^e = \dot{T}/J_0$, while bounding surface plasticity is used to describe the plastic response. The geosynthetic reinforcements in the present study were assumed to be Type A geosynthetics (Liu and Ling, 2007), for which the bounding lines on the tension side are expressed as

$$T_+ = A + \bar{J}_p\varepsilon^p \tag{II.2}$$

T_+ is the bounding loads per unit width, while A and $\bar{J}_p$ are model parameters. With the bounding lines, the plastic stiffness of geosynthetics is defined as

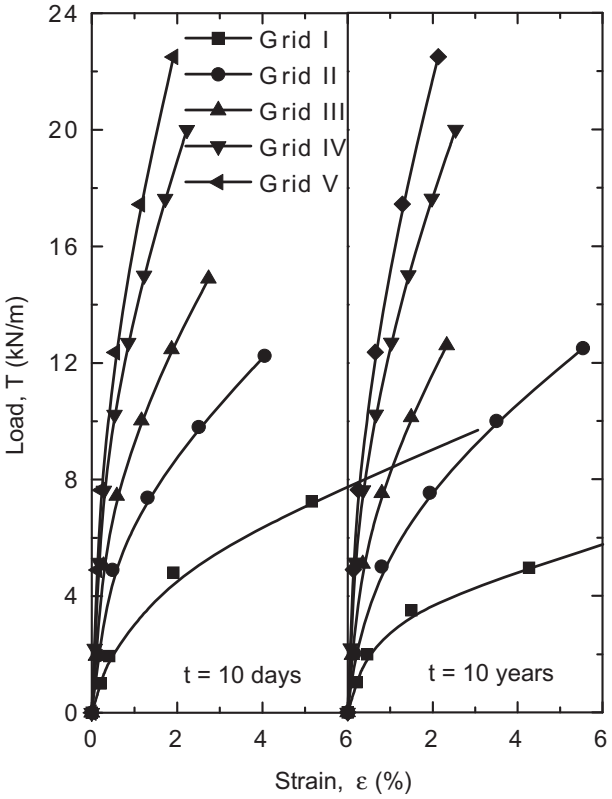

Fig. 14. Isochrones of geogrid reinforcements.

$$J_p = \frac{dT}{d\varepsilon^p} = \bar{J}_p + h_0^L\frac{\delta}{\delta_{in}-\delta} \tag{II.3}$$

where h_0^L is the hardening parameter, δ is the distance of the present stress state to the bounding line and δ_{in} is the initial distance at the beginning of loading path.

The viscoplastic behavior is assumed to follow Perzyna overstress theory. It is estimated that tertiary creep would not occur in the reinforcements for working stress condition, the static curve introduced for Type A geosynthetics in Liu and Ling (2005) is used for monotonic loading in this study

$$T_s = c_1\varepsilon^{c_2} \tag{II.4}$$

The viscoplastic strain rate is then defined as

$$\dot{\varepsilon}^{vp} = \frac{1}{\eta}|T-T_s|^n\mathrm{sign}(\dot{\varepsilon}), \quad T \geq T_s \tag{II.5}$$

where η is the viscous coefficient, $n = n_0[1+\exp(-\kappa\varepsilon^{vp})]$, and n_0 and κ are two model parameters.

Altogether 9 model parameters are needed to describe nonlinear, creep and stress relaxation behavior of Type A geosynthetic reinforcements, which are J_0, A, $\bar{J}_p$, h_0^L, c_1, c_2, n_0, κ, and η.

Table 3
Model parameters for geogrid reinforcements.

	J_e (kN/m)	A (kN/m)	$\bar{J}_p$ (kN/m)	h_0^L (kN/m)	c_1 (kN/m)	c_2 (kN/m)	n_0	κ	η (kN/m)$^{1/n}$
Grid I	500	240	15.4	76.9	20	0.52	3.8	14	2.2×10^9
Grid II	1300	240	40	200	52	0.52	3.8	14	2.2×10^9
Grid III	2000	240	64	320	83.2	0.52	3.8	14	2.2×10^9
Grid IV	3200	240	100	500	130	0.52	3.8	14	2.2×10^9
Grid V	4000	240	124	620	161.2	0.52	3.8	14	2.2×10^9

The model parameters for the five geogrids investigated in this study are given in Table 3, and their isochrones at $t = 14$ days and $t = 10$ years are shown in Fig. 14 (Liu and Won, 2009).

References

AASHTO, 2007. LRFD Bridge Design Specifications. American Association of State Highway and Transportation Officials (AASHTO), Washington, D.C.

Allen, T.M., Bathurst, R.J., 2002. Observed long-term performance of geosynthetic walls, and implications for design. Geosynthetics International 9 (5–6), 567–606.

Allen, T.M., Bathurst, R.J., Holtz, R.D., Walters, D., Lee, W.F., 2003. A new working stress method for prediction of reinforcement loads in geosynthetic walls. Canadian Geotechnical Journal 40 (5), 976–994.

Bathurst, R.J., Nernheim, A., Walters, D.L., Allen, T.M., Burgess, P., Saunders, D., 2009. Influence of reinforcement stiffness and compaction on the performance of four geosynthetic reinforced soil walls. Geosynthetics International 16 (1), 43–59.

Benjamim, C.V.S., Bueno, B.S., Zornberg, J.G., 2007. Field monitoring evaluation of geotextile-reinforced soil-retaining walls. Geosynthetics International 14 (2), 100–118.

Bergado, D.T., Teerawattanasuk, C., 2008. 2D and 3D numerical simulations of reinforced embankments on soft ground. Geotextiles and Geomembranes 26 (1), 39–55.

Chan, A.H.C., 1993. User Manual for Diana-Swandyne-II. Glasgow University, Glasgow, U.K.

Christopher, B.R., 1993. Deformation response and wall stiffness in relation to reinforced soil wall design. Ph.D. thesis, Purdue University, West Lafayette, Indiana.

Correia, A.A.S., Pinto, M.I.M., Lopes, M.L.C., 2011. Design brick faced retaining walls reinforced with geotextiles – face deformation. Journal of Geotechnical and Geoenvironmental Engineering ASCE. doi:10.1061/(ASCE)GT.1943-5606.0000613.

Ehrlich, M., Mitchell, J.K., 1994. Working stress design method for reinforced soil walls. Journal of Geotechnical and Geoenvironmental Engineering ASCE 120 (4), 625–645.

Elias, V., Christopher, B.R., Berg, R.R., 2001. Mechanically Stabilized Earth Walls and Reinforced Soil Slopes Design and Construction Guidelines. Report FHWANHI-00-043. Federal Highway Administration (FHWA), Washington, D.C.

Fannin, R.J., 2001. Long-term variations of force and strain in a steep geogrid-reinforced soil slope. Geosynthetics International 8 (1), 81–96.

Fukushima, S., Tatsuoka, F., 1984. Strength and deformation characteristics of saturated sand at extremely low pressures. Soils and Foundations 24 (4), 30–48.

Guler, E., Hamderi, M., Demirkan, M.M., 2007. Numerical analysis of reinforced soil-retaining wall structures with cohesive and granular backfills. Geosynthetics International 14 (6), 330–345.

Hatami, K., Bathurst, R.J., 2006. A numerical model for reinforced soil segmental walls under surcharge loading. Journal of Geotechnical and Geoenvironmental Engineering 132 (6), 673–684.

Helwany, M.B., Wu, J.T.H., 1997. Numerical model for analyzing long-term performance of geosynthetic-reinforced soil structures. Geosynthetics International 2 (2), 429–453.

Helwany, S.M.B., Reardon, G., Wu, J.T.H., 1999. Effects of backfill on the performance of GRS retaining walls. Geotextiles and Geomembranes 17 (1), 1–16.

Helwany, S.M.B., Wu, J.T.H., Kitsabunnarat, A., 2007. Simulating the behavior of GRS bridge abutments. Journal of Geotechnical and Geoenvironmental Engineering ASCE 133 (10), 1229–1240.

Hirakawa, D., Kongkitkul, W., Tatsuoka, F., Uchimura, T., 2003. Time dependent stress–strain behaviour due to viscous properties of geogrid reinforcement. Geosynthetics International 10 (6), 176–199.

Huang, C.C., Luo, W.M., 2010. Behavior of cantilever and geosynthetic-reinforced walls on deformable foundations. Geotextiles and Geomembranes 28 (5), 448–459.

Jewell, R.A., Milligan, G.W.E., 1989. Deformation calculations for reinforced soil walls. In: Proceedings of the 12th International Conference on Soil Mechanics and Foundation Engineering, Vol.2. Reio de Janerio, Brazil, pp. 1257–1262.

Kaliakin, V.N., Dechasakulsom, M., Leshchinsky, D., 2000. Investigation of the isochrone concept for predicting relaxation of geogrids. Geosynthetics International 7 (2), 79–99.

Karpurapu, R., Bathurst, R.J., 1995. Behaviour of geosynthetic reinforced soil retaining walls using the finite element method. Computers and Geotechnics 17 (3), 279–299.

Klar, A., Sas, T., 2009. Rational approach for the analysis of segmental reinforced soil walls based on kinematic constraints. Geotextiles and Geomembranes 27 (5), 332–340.

Kongkitkul, W., Hirakawa, D., Tatsuoka, F., Uchimura, T., 2004. Viscous deformation of geosynthetic reinforcement under cyclic loading conditions and its model simulation. Geosynthetics International 11 (2), 73–99.

Kongkitkul, W., Tatsuoka, F., Hirakawa, D., 2007. Creep rupture curve for simultaneous creep deformation and degradation of geosynthetic reinforcement. Geosynthetics International 14 (4), 189–200.

Kongkitkul, K., Tatsuoka, F., Hirakawa, D., Sugimoto, T., Kawahata, S., Ito, M., 2010. Time histories of tensile force in geogrid arranged in two full-scale high walls. Geosynthetics International 17 (1), 12–32.

Lee, K.L., Seed, H.B., 1967. Drained characteristics of sand. Journal of Soil Mechanics and Foundations Division 93 (6), 117–141.

Leshchinsky, D., Vulova, C., 2001. Numerical investigation of the effects of geosynthetic spacing on failure mechanisms in MSE block walls. Geosynthetics International 8 (4), 343–365.

Leshchinsky, D., 2009. On global equilibrium in design of geosynthetic reinforced walls. Journal of Geotechnical and Geoenvironmental Engineering ASCE 135 (3), 309–315.

Li, A.L., Rowe, R.K., 2001. Influence of creep and stress-relaxation of geosynthetic reinforcement on embankment behavior. Geosynthetics International 8 (3), 233–270.

Li, A.L., Rowe, R.K., 2008. Effects of viscous behaviour of geosynthetic reinforcement and foundation soils on embankment performance. Geotextiles and Geomembranes 26 (4), 317–334.

Li, F.L., Peng, F.L., Tan, Y., Kongkitkul, W., Siddiquee, M.S.A., 2011. FE simulation of viscous behavior of geogrid-reinforced sand under laboratory-scale plane-strain-compression testing. Geotextiles and Geomembranes. doi:10.1016/j.geotexmem.2011.09.005.

Ling, H.I., Leshchinsky, D., 2003. Finite element parametric studies of the behavior of segmental block reinforced soil retaining walls. Geosynthetics International 10 (3), 77–94.

Ling, H.I., Liu, H., 2003. Pressure-level dependency and densification behavior of sand through a generalized plasticity model. Journal of Engineering Mechanics ASCE 129 (8), 851–860.

Ling, H.I., Liu, H., Kaliakin, V.N., Leshchinsky, D., 2004. Analyzing dynamic behavior of geosynthetic-reinforced soil retaining walls. Journal of Engineering Mechanics ASCE 130 (8), 911–920.

Ling, H.I., Liu, H., Mohri, Y., 2005. Parametric studies on the behavior of reinforced soil retaining walls under earthquake loading. Journal of Engineering Mechanics ASCE 131 (10), 1056–1065.

Ling, H.I., Liu, H., 2009. Deformation analysis of reinforced soil retaining walls – simplistic versus sophisticated finite element analyses. Acta Geotechnica 4, 203–213.

Liu, H., 2002. Finite element simulation of the response of geosynthethic-reinforced soil walls. PhD thesis, Columbia Univ., New York.

Liu, H., Ling, H.I., 2005. Constitutive modeling of the time-dependent monotonic and cyclic behavior of geosynthetics. In: Ling, H.I. (Ed.), Geosynthetics and Geosynthetic-Engineered Soil Structures. Columbia University, New York, NY, pp. 281–302.

Liu, H., Ling, H.I., 2007. A unified elastoplastic–viscoplastic bounding surface model of geosynthetics and its applications to GRS-RW analysis. Journal of Engineering Mechanics ASCE, 801–815.

Liu, H., Wang, X., Song, E., 2009. Long-term behavior of GRS retaining walls with marginal backfill soils. Geotextiles and Geomembranes 27 (4), 295–307.

Liu, H., Won, M.S., 2009. Long-term reinforcement load of geosynthetic-reinforced soil retaining walls. Journal of Geotechnical and Geoenvironmental Engineering ASCE 135 (7), 875–889.

Onodera, S., Fukuda, N., Nakane, A., 2004. Long-term behavior of geogrid reinforced soil walls. In: Proceedings 3rd Geosynthetics Asia, Seoul, Korea, pp. 255–264.

Rowe, R.K., Ho, S.K., 1998. Horizontal deformation in reinforced soil walls. Canadian Geotechnical Journal 35 (2), 312–327.

Rowe, R.K., Skinner, G.D., 2001. Numerical analysis of geosynthetic reinforced retaining wall constructed on a layered soil foundation. Geotextiles and Geomembranes 19 (7), 387–412.

Rowe, R.K., Taechakumthorn, C., 2008. Combined effect of PVDs and reinforcement on embankments over rate-sensitive soils. Geotextiles and Geomembranes 26 (3), 239–249.

Rowe, R.K., Taechakumthorn, C., 2011. Design of reinforced embankments on soft clay deposits considering the viscosity of both foundation and reinforcement. Geotextiles and Geomembranes 29 (5), 448–461.

Skinner, G.D., Rowe, R.K., 2003. Design and behaviour of geosynthetic reinforced soil walls constructed on yielding foundations. Geosynthetics International 10 (6), 200–214.

Skinner, G.D., Rowe, R.K., 2005. Design and behaviour of a geosynthetic reinforced retaining wall and bridge abutment on a yielding foundation. Geotextiles and Geomembranes 23 (3), 235–260.

Viswanadham, B.V.S., König, D., 2009. Centrifuge modeling of geotextile-reinforced slopes subjected to differential settlements. Geotextiles and Geomembranes 27 (2), 77–88.

Wu, J.T.H., Helwany, S.M.B., 1996. A performance test for assessment of long-term creep behavior of soil–geosynthetic composites. Geosynthetics International 3 (1), 107–124.

Yang, G., Zhang, B., Lv, P., Zhou, Q., 2009. Behaviour of geogrid reinforced soil retaining wall with concrete-rigid facing. Geotextiles and Geomembranes 27 (5), 350–356.

Yeo, S.S., Hsuan, Y.G., 2010. Evaluation of creep behavior of high density polyethylene and polyethylene-terephthalate geogrids. Geotextiles and Geomembranes 28 (5), 409–421.

Yoo, C., Kim, S.B., 2008. Performance of a two-tier geosynthetic reinforced segmental retaining wall under a surcharge load: full-scale load test and 3D finite element analysis. Geotextiles and Geomembranes 26 (6), 460–472.

B / >.C #D? ? @?’ A